Bioresorbable Bilayered Elastomer/Hydrogel Constructs with Gradual Interfaces for the Fast Actuation of Self-Rolling Tubes

Mathilde Grosjean, Sidzigui Ouedraogo, Stéphane Déjean, Xavier Garric, Valeriy Luchnikov, Arnaud Ponche, Noelle Mathieu, Karine Anselme, Benjamin Nottelet

ACS APPLIED MATERIALS & INTERFACES

www.acsami.org

Research Article

Bioresorbable Bilayered Elastomer/Hydrogel Constructs with Gradual Interfaces for the Fast Actuation of Self-Rolling Tubes

Mathilde Grosjean, Sidzigui Ouedraogo, Stéphane Déjean, Xavier Garric, Valeriy Luchnikov, Arnaud Ponche, Noëlle Mathieu, Karine Anselme, and Benjamin Nottelet*

Cite This: *ACS Appl. Mater. Interfaces* 2022, 14, 43719–43731

Read Online

ACCESS | Metrics & More | Article Recommendations | Supporting Information

ABSTRACT: In the biomedical field, self-rolling materials provide interesting opportunities to develop medical devices suitable for drug or cell encapsulation. However, to date, a major limitation for medical applications is the use of non-biodegradable and non-biocompatible polymers that are often reported for such applications or the slow actuation witnessed with degradable systems. In this work, biodegradable self-rolling tubes that exhibit a spontaneous and rapid actuation when immersed in water are designed. Photo-crosslinkable hydrophilic and hydrophobic poly(ethylene glycol)-poly(lactide) (PEG-PLA) star-shaped copolymers are prepared and used to prepare bilayered constructs. Thanks to the discrete mechanical and swelling properties of each layer and the cohesive/gradual nature of the interface, the resulting bilayered films are able to self-roll in water in less than 30 s depending on the nature of the hydrophilic layer and on the shape of the sample. The cytocompatibility and degradability of the materials are demonstrated and confirm the potential of such self-rolling resorbable biomaterials in the field of temporary medical devices.

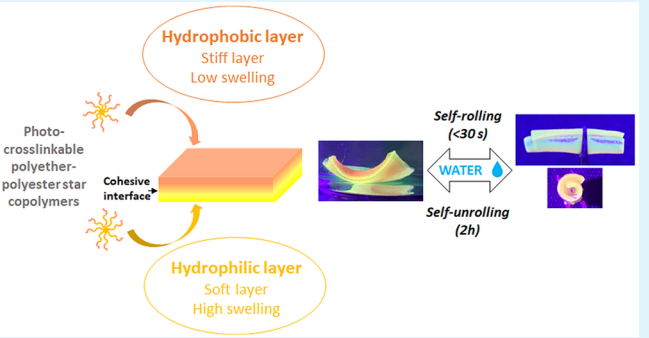

KEYWORDS: *self-rolling, actuation, star copolymer, hydrogel, elastomer, degradable network, polylactide, poly(ethylene glycol)*

1. INTRODUCTION

In the frame of biomedical applications, biomaterials that can undergo a morphological or mechanical transition in response to a stimulus are highly sought after. Shape memory materials and reversibly swelling hydrogels or actuators[1−5] are examples of such biomaterials that find applications in the frame of medical devices, diagnostics, or drug delivery. In this context, self-rolling tubes provide interesting opportunities to design spatially constrained medical devices suitable for the encapsulation of drugs or cells. Nevertheless, in most examples, the use of non-biodegradable and non-biocompatible materials is reported,[6,7] which constitutes a major limitation for medical applications. Moreover, the stimuli that can be used to activate the rolling of the films are limited. For example, shape changes in response to temperature[8−12] and pH[13,14] are common but not always suitable due to the sensibility of cells or active molecules. In this context, triggering the spontaneous rolling of a flat film by simple swelling in water appears to be very attractive. Such self-rolling systems rely on the use of bilayered films, where each layer presents different swelling behaviors and/or mechanical properties. These inhomogeneities in the normal direction of the films yield different volumetric responses of the distinct layers and an inhomogeneous stress profile in the normal direction, which ultimately generates the bending moment.[15]

Though conceptually simple, the actuation of degradable polymeric bilayer constructs based on the differential swelling of the two layers remains rare. One example reported the use of a polysuccinimide (PSI)/polycaprolactone (PCL) bilayer. Tubes were formed in physiological buffer due to the hydrolysis of PSI, which led to the in situ formation of water-swellable polyaspartic acid. In this case, rolling was relatively slow with over 9 h to form the targeted tube.[16] Another study displayed a folded bilayered film made of crosslinked gelatin and a hydrophobic PCL polymer that can self-roll by immersion in PBS at 37 °C in 25 min.[17] However, folding was not reversible and not uniform, which ultimately led to half cylinders and not tubes. Finally, self-rolling of electrospun PLA/PCL bilayers was reported. The irreversible formation of tubes took place in water in 5 min at 40 °C due to the temperature-induced relaxation of intrinsic stress in the PLA porous mat.[18]

Received: June 27, 2022
Accepted: September 8, 2022
Published: September 19, 2022

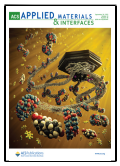

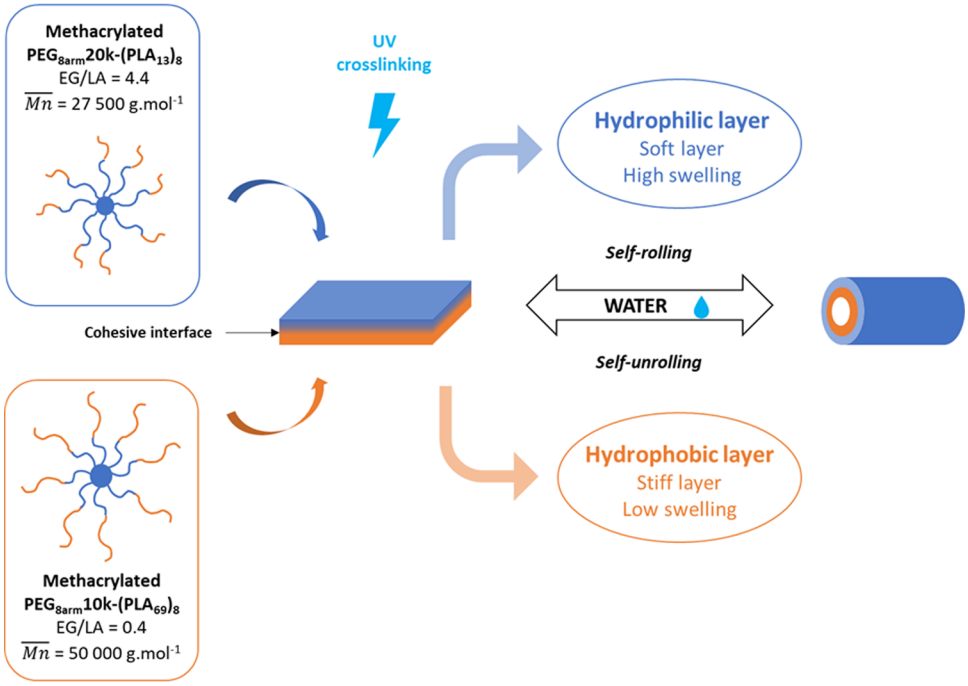

Figure 1. Schematic representation of the bilayered construct preparation and self-rolling.

Since the rolling of the tube depends on various factors, such as the thickness of the layers, the Young's modulus, the bending stiffness, or the affinity for a solvent,[15] one major challenge in the design of bilayer polymer films is the choice of the polymers. Indeed, the polymers should have different properties to induce a structural inhomogeneity in the film but a good affinity to ensure cohesion between the layers and an efficient transfer of stresses in the construct.

In this paper, we report on the fabrication of biodegradable bilayer tubes based on poly(ethylene glycol)-poly(lactide) (PEG-PLA) UV-crosslinkable eight-armed star-shaped copolymers. By varying the polyether−polyester ratio, a family of copolymers with similar morphologies and close chemical compositions but different mechanical and swelling properties is obtained. These hydrophilic and hydrophobic copolymers are characterized prior to their use to form bilayered constructs. A covalent association between the two layers is provided through photo-crosslinking to ensure the absence of delamination and an efficient transfer of forces to ensure a fast self-rolling process. We demonstrate that the optimized bilayered constructs display spontaneous and rapid rolling in less than 30 s when immersed in water, thanks to the higher swelling of the hydrophilic layer (H^+L) compared to the limited swelling of the hydrophobic layer (H^-L) (Figure 1). The cytocompatibility and degradability are finally assessed to further confirm the applicability of these self-rolling tubes in the field of temporary medical devices.

2. MATERIALS AND METHODS

2.1. Materials. D,L-Lactide, D-lactide, and L-lactide were purchased from Corbion (Gorinchem, The Netherlands). Hydroxyl-terminated eight-armed poly(ethylene glycol) (tripentaerythritol) (PEG_{8arm}10k, M_w = 10 000 g mol^{-1} and PEG_{8arm}20k, M_w = 20 000 g mol^{-1}) was purchased from JenKem Technology Co., Ltd (Beijing, China). Tin(II) 2-ethylhexanoate ($Sn(Oct)_2$), toluene, dichloromethane (DCM), *N*,*N*-dimethylformamide (DMF), triethylamine (Et_3N), methacryloyl chloride, fluorescein isothiocyanate (FITC), rhodamine B isothiocyanate, Celite 545, diethyl ether (Et_2O), ethanol (EtOH), tetrahydrofuran (THF), and acetone were purchased from Sigma-Aldrich (St Quentin Fallavier, France). All chemicals were used without further purification with the exception of toluene and DCM, which were dried over calcium hydride and freshly distilled before use.

2.2. Characterization. Average molecular weights($\bar{M}_n$) and dispersities ($Đ$) were determined by size-exclusion chromatography (SEC, Shimadzu SIL-20A HT) using two mixed medium columns PLgel 5 μm MIXED-C (300 mm × 7.8 mm), a Shimadzu RI detector 20A, and a Shimadzu UV detector SPD-20A (260 and 290 nm) (40 °C thermostatic analysis cells). THF was used as a mobile phase in isocratic mode with a flow rate of 1 mL min^{-1} at 30 °C (column temperature). The polymer was dissolved in THF to reach 5 mg mL^{-1} concentration; afterward, the solution was filtered through a 0.45 μm Millipore filter before injection. $\bar{M}_n$ and $Đ$ were expressed according to calibration using polystyrene standards.

^{1}H nuclear magnetic resonance (NMR) spectra were recorded at the Laboratoire de Mesures Physiques (LMP) of the University of Montpellier (UM) using a Bruker Avance III HD 400 MHz spectrometer (Bruker, Fällanden, Switzerland) and were calibrated to TMS on the basis of the relative chemical shift of the solvent used as an internal standard. ^{1}H two-dimensional (2D) diffusion-ordered (DOSY) NMR spectra were recorded on a Bruker Avance III 600 (Bruker, Fällanden, Switzerland) spectrometer equipped with a 5 mm TCI Prodigy Z-gradient cryoprobe. A standard gradient amplifier (GREAT 1/10-E) generates a maximum gradient strength of 65.7 Gauss cm^{-1} at a current of 10 A. The gradient strengths were calibrated using a sample of D_2O 99.96% deuterated from Eurisotop (Saint−Aubin, France). Diffusion measurement was performed with double stimulated echo and bipolar gradient pulses for convection compensation and Eddy current delay (dstebpgp) in a pseudo-2D mode and processed with the Bruker software T1/T2 package from Topspin 3.6.2 (Bruker). For this experiment, 16 dummy scans and 32 scans were used with a relaxation delay of 3 s. Diffusion time Δ was fixed to 0.3 s and gradient strength δ to 2.8 ms. Sinusoidal shapes were used for the gradients, and a linear gradient ramp with 16 increments between 2 and 95% was applied for the diffusion relevant gradients. The diffusion coefficients were calculated with the Bruker software package T1/T2 from Topspin 3.6.2 (Bruker). All diffusion coefficients were within an error range of ±5%.

^{1}H high-resolution magic-angle spinning (HRMAS) NMR experiments were carried out on a Varian VNMRS 600 MHz spectrometer.

https://doi.org/10.1021/acsami.2c11264
ACS Appl. Mater. Interfaces 2022, 14, 43719−43731

The samples were placed into a 4 mm quartz zirconia HRMAS rotor before the solvent was injected. Analyses were performed at 20 °C. The spectra were recorded at a spectral width of 7 kHz and a transmitter frequency offset of 600 Hz. Sixteen scans were used with an acquisition time of 1.14 s, a relaxation delay of 1 s, and a 30° pulse (3.92 μs).

For all of the NMR analyses, the solvent used was deuterated chloroform.

Thermal properties of the polymers were analyzed by differential scanning calorimetry (DSC) using a Mettler Toledo DSC 3 STAR system instrument. Analyses were carried out under a nitrogen atmosphere. Samples were heated from 0 to 100 °C (10 °C min^{-1}) and then cooled to −80 °C (10 °C min^{-1}) before a second heating ramp to 200 °C (5 °C min^{-1}). The glass-transition temperature (T_g) or melting temperature (T_m) was measured on the second heating ramp.

Fourier transform infrared (FTIR) spectra of polymer films were recorded with a Nicolet iS50 FTIR spectrometer (Thermo Scientific).

Scanning electron microscopy (SEM) images were recorded using a JEOL JSM-7900F microscope.

2.3. Synthesis of Copolymers. For the sake of clarity, the copolymers are named as follows: PLA corresponds to PD,L-LA (*aka* PLA50, 50% of L and D units), PDLA corresponds to PDLA (*aka* PLA0, 100% D units), and PLLA corresponds to PLLA (*aka* PLA100, 100% L units). PLA_x corresponds to PLA blocks with a degree of polymerization DPn = x.

Copolymers are named as follows: PEG_{8arm}*y*k-$(PLA_x)_z$, where y corresponds to the molecular weight of the PEG macroinitiator, x corresponds to the degree of polymerization DPn of the PLA block, and z corresponds to the number of PLA blocks per copolymer. It is worth noting that the addition of MC at the end of the denomination corresponds to the copolymers functionalized by methacrylate groups.

Crosslinked networks obtained from the copolymers are named as follows: PEG_{8arm}*Y*k-PLA*X*k, where Y corresponds to the molecular weight of PEG and X corresponds to the overall molecular weight of PLA in the copolymer used to form the corresponding networks.

2.3.1. PEG_{8arm}10k-$(PLA_{69})_8$. A star-shaped copolymer, PEG_{8arm}-10k-$(PLA_{69})_8$, was synthesized by bulk ring-opening polymerization (ROP). For this, determined amounts of D,L-lactide and PEG_{8arm}10k were introduced in a flask, to which $Sn(Oct)_2$ was then added (0.1 mol % with respect to OH groups). Argon-vacuum cycles were applied before sealing the flask under vacuum. ROP was carried out in bulk in an oven at 130 °C for 5 days under constant stirring. Afterward, the mixture was dissolved in DCM and precipitated in cold EtOH. The final copolymer was dried under reduced pressure to constant mass.

2.3.2. PEG_{8arm}20k-$(PLA_{13})_8$, PEG_{8arm}20k-$(PDLA_{13})_8$, and PE-G_{8arm}20k-$(PLLA_{13})_8$. Star-shaped copolymers PEG_{8arm}20k-$(PLA_{13})_8$ were synthesized by ROP in solution. For this, determined amounts of D,L-lactide, PEG_{8arm}20k, and $Sn(Oct)_2$ (0.1 mol % with respect to OH groups) were introduced into a flask and solubilized in toluene (30% w/v). ROP was carried out at 100 °C for 24 h under an argon atmosphere and constant stirring. Afterward, the mixture was concentrated before being purified by precipitation in cold Et_2O. The final copolymer was recovered by filtration and dried under reduced pressure to constant mass. PEG_{8arm}20k-$(PDLA_{13})_8$ and PEG_{8arm}20k-$(PLLA_{13})_8$ were prepared similarly, using D-lactide and L-lactide, respectively.

^{1}H NMR (400 MHz; $CDCl_3$): δ (ppm) = 5.1 (q, 1H, CO-C$\underline{H}$-(CH_3)-O), 4.3 (m, 2H, O-CH_2-C-C$\underline{H}_2$-O), 4.3 (m, 1H, C$\underline{H}$-OH), 3.8 (m, 2H, O-C$\underline{H}_2$-C-CH_2-O), 3.6 (s, 4H, C$\underline{H}_2$-C$\underline{H}_2$-O), 1.5 (t, 3H, CO-CH-(C$\underline{H}_3$)-O) (Figure S1)

The copolymer molecular weight was determined using eqs (1) and (2) using a molecular mass of 72 g mol^{-1} for the lactic unit.

$$\overline{DP}_{PLA} = \overline{DP}_{PEG} \times \left(\frac{I_{5.1\ PLA\ peak\ integration}}{I_{3.6\ PEG\ peak\ integration}} \right) \quad (1)$$

$$\bar{M}_n = 8 \times (\overline{DP}_{PLA} \times 72) + \bar{M}_{n_{PEG\ 8\ arm}} \quad (2)$$

2.4. Methacrylate Functional Copolymers. *2.4.1. PEG_{8arm}10k-$(PLA_{69})_8$-MC.* The eight-armed star-block copolymer PEG_{8arm}10k-$(PLA_{69})_8$ was solubilized in freshly distilled DCM (10% w/v). Determined amounts of Et_3N (20 equiv/OH group) were added. The mixture was then cooled at 0 °C before adding methacryloyl chloride with a dropping funnel (20 equiv/OH group). After 2 h, the mixture was heated to 50 °C for 72 h under stirring in the dark. Then, the reaction medium was filtered on Celite 545 before being washed with distilled water and concentrated. Afterward, the mixture was precipitated in cold EtOH. The methacrylate functional PE-G_{8arm}10k-$(PLA_{69})_8$-MC was dried under reduced pressure to constant mass.

2.4.2. PEG_{8arm}20k-$(PLA_{13})_8$-MC, PEG_{8arm}20k-$(PDLA_{13})_8$-MC, and PEG_{8arm}20k-$(PLLA_{13})_8$-MC. A similar procedure to that described above was used to prepare methacrylate functional PEG_{8arm}20k-$(PLA_{13})_8$-MC, PEG_{8arm}20k-$(PDLA_{13})_8$-MC, and PEG_{8arm}20k-$(PLLA_{13})_8$-MC. The only difference was the use of lower amounts of Et_3N (5 equiv/OH group) and methacryloyl chloride (5 equiv/OH group). The precipitation was done in cold Et_2O instead of cold EtOH.

The functionalization was confirmed by ^{1}H NMR and DOSY NMR.

The yield of functionalization was determined by comparing the integration of the methacrylate characteristic signal at 6.2 and 5.6 ppm and the integration of proton resonance at 3.6 ppm.

^{1}H NMR (400 MHz; $CDCl_3$): δ (ppm) = 6.2 (d, 1H, CO-C(CH_3)=C$\underline{H}_2$), 5.6 (d, 1H, CO-C(CH_3)=C$\underline{H}_2$), 5.1 (q, 1H, CO-C$\underline{H}$-(CH_3)-O), 4.3 (m, 2H, O-CH_2-C-C$\underline{H}_2$-O), 4.3 (m, 1H, C$\underline{H}$-OH),), 3.8 (m, 2H, O-C$\underline{H}_2$-C-CH_2-O), 3.6 (s, 4H, C$\underline{H}_2$-C$\underline{H}_2$-O, 1.8 (t, 3H, CO-C(C$\underline{H}_3$)=CH_2), 1.5 (t, 3H, CO-CH-(C$\underline{H}_3$)-O).

2.5. Film Preparation, Photo-crosslinking, and Gel Fraction. Polymer films were prepared by the solvent evaporation method. The copolymers were first solubilized in DCM (10% w/v). Then, the solutions were slowly dried in a dark place in an aluminum mold to obtain thin films, which were further dried under vacuum for 24 h.

The resulting films were irradiated under UV light (5 min per side) using a Dymax PC-2000 system equipped with a metal halide bulb (75 mW/cm^2). The distance measured between the bulb and samples was 13.5 cm.

Afterward, samples were cut (10 mm × 10 mm), weighed, and placed in DCM (5 mL). After 24 h, the insoluble crosslinked parts were removed from DCM and dried under vacuum. Finally, the samples were weighed to determine the gel fraction according to eq (3). The experiment was run in triplicate.

$$\text{gel fraction}(\%) = \frac{\text{weight of insoluble crosslinked parts}}{\text{weight of initial sample}} \times 100 \quad (3)$$

2.6. Water Uptake. Samples were cut (10 mm × 10 mm), weighed (W_i = initial weight), and placed in 5 mL of phosphate-buffered saline (PBS) (pH 7.4) at 37 °C under stirring. At different time points, samples were removed from PBS and weighed (W_w = weight of the wet samples after w time in PBS). The water uptake of the samples was calculated from eq (4). The experiment was run in triplicate.

$$\text{water uptake}(\%) = \frac{W_w - W_i}{W_i} \times 100 \quad (4)$$

2.7. Mechanical Properties. *2.7.1. Tensile Tests.* Dog-bone strips were stamped from polymer films, and their thickness was measured with a micrometer. The mechanical properties were assessed at room temperature on dog-bone strips (10 mm × 2 mm) with an Instron 3344 testing machine equipped with a 500 N load cell at a deformation rate of 10 mm min^{-1}.

Tensile properties were also evaluated in the hydrated state following the above method. Samples were hydrated during 6 h before the tensile tests and were tested on the same testing machine equipped with a BioPuls Bath accessory at 37 °C in deionized water.

https://doi.org/10.1021/acsami.2c11264
ACS Appl. Mater. Interfaces 2022, 14, 43719−43731

Young's modulus (E, MPa), stress at yield (σ_{yield}, MPa), strain at yield (ε_{yield}, %), stress at break (σ_{break}, MPa), and strain at break (ε_{break}, %) were expressed as the mean value of three measurements.

2.7.2. Cyclic Loads. The samples were elongated to 15% and subsequently let to recover (0%) before immediately being stretched again to 15% (nine cycles). To evaluate the ability of the material to deform reversibly without loss of energy, the resilience was calculated according to eq (5). It was calculated from the value of the ninth cycle. The same tests were repeated with deformation of 5 and 2%.

$$\text{resilience}\ (\%) = \frac{\text{area under unloading curve}}{\text{area under loading curve}} \times 100 \quad (5)$$

Resilience (%) was expressed as the mean of three measurements.

2.7.3. Relaxation. The sample was elongated to 15%. During 800 s, the strength needed to maintain the constant elongation was monitored. To evaluate the capacity of the materials to release the mechanical stress under constant deformation, the relaxation was calculated according to eq (6). The same tests were repeated with deformation of 10, 5, and 2%.

$$\text{relaxation}(\%) = \frac{\text{initial strength}}{\text{final strength}} \times 100 \quad (6)$$

Relaxation (%) was expressed as the mean of three measurements.

2.8. Bilayered Construct Preparation and Self-Rolling. Bilayer constructs were prepared by the association of two polymer films. The first layer was prepared from solvent evaporation. The corresponding copolymer was first solubilized in DCM. Then, the solution was slowly dried in a dark place in an aluminum mold to obtain a film. Afterward, the second polymer was solubilized in DCM, and the resulting solution was dropped over the first layer. After the evaporation of the solvent, the bilayer construct was further dried under vacuum for 24 h before being exposed to UV light (5 min per side) using a Dymax PC-2000 system equipped with a metal halide bulb.

To study their spontaneous rolling, samples were cut and immersed in water at 37 °C. The self-rolling was monitored visually.

2.9. Degradation Study. Samples were cut (10 mm × 10 mm), weighed (W_i = initial weight), and placed in 5 mL of PBS (pH 7.4) at 37 °C under stirring. At different time points, samples were removed from PBS and dried to constant mass (W_x = dry weight after x time in PBS). The remaining mass of the samples was calculated from eq (7). The experiment was run in triplicate.

$$\text{remaining mass}(\%) = \frac{W_x}{W_i} \times 100 \quad (7)$$

2.10. Cytotoxicity Assay. Cells and control polymers films were chosen following ISO 10993-5 guidelines. Mouse fibroblast L929 cells (ECACC 85 011 425) were maintained in DMEM high glucose supplemented with 5% fetal bovine serum (FBS), 1% L-glutamine, and 1% penicillin/streptomycin and cultured at 37 °C and 5% CO_2. Cells were tested to be free of mycoplasms. Negative (RM-C high-density polyethylene, denoted C−) and positive (RM-B 0.25% zinc dibutyldithiocarbamate (ZDBC) polyurethane, denoted C+) control films were purchased from the Hatano Research Institute (Ochiai 729-5, Hadanoshi, Kanagawa 257, Japan). Cytotoxicity was assessed on extracts. Extractions were carried out at 6 cm^2 of polymer film per mL for 24 h at 37 °C under sterile conditions in complete growth medium, following ISO 10993-12 recommendations. Films were irradiated under UV light for 5 min for sterilization. L929 cells were seeded at 10 × 10^3 cells per well in a 96-well plate and allowed to attach overnight. The culture medium was then removed and discarded from the cultures, and an aliquot of the film extract was added into each well. After 24 h of incubation under an appropriate atmosphere, extract cytotoxicity was assessed using the CellTiter-Glo Luminescent Cell Viability Assay, according to the manufacturer's instruction. Briefly, 50 μL of medium from each well was removed, followed by the addition of the same volume of CellTiter-Glo. After 10 min of incubation at room temperature, luminescence was measured using a CLARIOstar microplate reader (BMG LABTECH's) to quantify the ATP present.

2.11. Statistical Analysis. The data are shown as the mean ± standard deviation (SD), and when applicable, the statistical difference of the results was evaluated using R software. For nonparametric data, results were analyzed using a Kruskal−Wallis test followed by a Dunn post-hoc test (threshold of significance $^*p < 0.05$).

3. RESULTS AND DISCUSSION

3.1. Synthesis of Methacrylate Functional Copolymers. Various star-shaped copolymers based on a similar structure composed of a polyether core and polyester side arms were synthesized to meet the properties required to get the targeted self-rolling tubes. First, eight-armed copolymers were chosen to generate crosslinked networks as star-shaped copolymers exhibit improved mechanical properties compared to their linear counterparts.[19] Moreover, the higher number of chain ends guarantees multifunctionalization of the copolymers with UV-reactive moieties leading to high crosslinking efficiencies without the use of toxic photoinitiators. Second, as spontaneous rolling is the consequence of a structural inhomogeneity of the films in the normal direction,[15] it was chosen to develop tubes composed of two layers with different mechanical and swelling properties, namely, a hydrophilic layer (H^+L) and a hydrophobic layer (H^-L). To allow this variation of hydrophilicity and stiffness while ensuring the compatibility and interfacial cohesion between the two layers, we chose to work with polymers based on polyether central blocks associated with side blocks of polyesters in a star-shaped topology. Hence, various polymers that differed not only by their mechanical properties but also by their affinity for water were designed by adjusting the polyether−polyester ratio in the star copolymers.

Four copolymers were obtained and could be sorted into two categories, corresponding to the two layers of the tube. On the one hand, the first category is composed of PEG_{8arm}10k-$(PLA_{69})_8$ that is hydrophobic because of its high PLA content (EG/LA = 0.4). On the other hand, the second category gathers different copolymers that can lead to hydrogels thanks to their high content of PEG (EG/LA = 4.4). With the objective to tune the properties of the hydrophilic layer, three copolymers based on the three isomers of LA were synthesized. First, PEG_{8arm}20k-$(PLA_{13})_8$ was obtained from D,L-lactide. Then, crystalline PEG_{8arm}20k-$(PLLA_{13})_8$ and PEG_{8arm}20k-$(PDLA_{13})_8$ were prepared from L-lactide and D-lactide, respectively. Thanks to these different polymers, several materials that differ in terms of mechanical properties, degree of hydration, swelling in water, and degradation could be prepared to optimize the preparation of the bilayer construct and reach optimal self-rolling.

All of the copolymers were prepared by ROP from eight-armed hydroxy-terminated PEG and lactide, according to procedures of the literature.[20,21] Targeted and experimental molecular weights were in good agreement as confirmed by ^{1}H NMR spectra (Table 1). Low dispersities below 1.2 were determined by SEC analysis, which demonstrated the good control of polymerizations.

The star-block copolymers were further reacted with methacryloyl chloride to yield methacrylate functional star-shaped PEG-PLA copolymers. Methacrylation was preferred over acrylation in this work due to the high extent of crosslinking obtained with methacrylated star copolymers,

https://doi.org/10.1021/acsami.2c11264
ACS Appl. Mater. Interfaces 2022, 14, 43719−43731

Table 1. Molecular Weight and Dispersity of the Star-Shaped Copolymers

copolymer	$\bar{M}_{n_{theo}}$ (g mol^{-1})	$\bar{M}_{n_{NMR}}$ (g mol^{-1})	$Đ$	targeted layer
$PEG_{8arm}10k$-$(PLA_{69})_8$	50 000	53 100	1.2	hydrophobic
$PEG_{8arm}20k$-$(PLA_{13})_8$	27 500	27 500	1.1	hydrophilic
$PEG_{8arm}20k$-$(PLLA_{13})_8$	27 500	27 600	1.1	
$PEG_{8arm}20k$-$(PDLA_{13})_8$	27 500	26 600	1.1	

without the stability, and uncontrolled crosslinking witnessed with acrylated star copolymers (crosslinking upon storage, unwanted crosslinking during manipulation). The procedures were adapted between the hydrophobic and hydrophilic copolymers to avoid PLA degradation during functionalization. The experimental molecular weights calculated from the ^{1}H NMR spectra (Table 2) and the dispersities determined by SEC analysis (Figure S2) confirmed the absence of degradation at this step.

Table 2. Molecular Weight, Dispersity, and Thermal Properties of the Methacrylate Functional Star-Shaped Copolymers

copolymer	$\bar{M}_{n_{NMR}}$ (g mol^{-1})	$Đ$	T_g (°C)	T_m (°C)	ΔH_m (J g^{-1})
$PEG_{8arm}10k$-$(PLA_{69})_8$-MC	52 400	1.2	11.8	nd[a]	nd
$PEG_{8arm}20k$-$(PLA_{13})_8$-MC	27 500	1.1	nd	33.0	−48.2
$PEG_{8arm}20k$-$(PLLA_{13})_8$-MC	27 600	1.1	nd	38.6	−50.4
$PEG_{8arm}20k$-$(PDLA_{13})_8$-MC	26 700	1.1	nd	39.1	−63.3

[a]Not detected under the conditions of analysis.

Typical ^{1}H NMR spectra of methacrylate functional eight-armed star-shaped PEG-PLA copolymers are shown in Figure S3. Peaks at 6.2 and 5.6 ppm (peaks a and b) correspond to alkene protons of the methacrylate chain end, whereas the peak at 1.8 ppm (peak c) corresponds to the methyl groups. The peaks at 5.1 ppm (peak d) and 1.5 ppm (peak e) correspond to the methine and methylene groups of the PLA backbone, respectively. The peaks at 4.3 ppm (peak g) were attributed to both the tripentaerythritol core and the (OH) terminal of the copolymers. Finally, the peak at 3.6 ppm (peak f) was assigned to the methylene groups of PEG. By comparison between the integration of the peaks of the methylene groups of PEG and of the methacrylate chain ends, a functionalization degree of 100% was calculated for all of the methacrylated copolymers.

The grafting of methacrylate functions onto star-shaped PEG-PLA chain ends was further confirmed by ^{1}H DOSY NMR since methacrylate signals displayed a reduced coefficient of diffusion after grafting and are aligned with the signals of the copolymer backbone (Figure S4).

These results confirmed the successful chain-end functionalization of star-shaped PEG-PLA with methacrylate moieties that will allow the preparation of UV-photo-crosslinkable materials and ensure a covalent association and cohesion between the layers in the final construct.

3.2. Photo-crosslinking and Swelling Behavior.

Methacrylated star copolymers were used to prepare crosslinked networks. To evaluate their potential to be used as a component of the bilayer tube, each material was first investigated individually in terms of gel fraction, swelling, and mechanical properties (see the next section). For this purpose, polymer films were prepared by solvent casting.

Four samples were studied (Figure 2). In the hydrophobic category, PEG_{10k}-PLA_{40k} was obtained from $PEG_{8arm}10k$-$(PLA_{69})_8$-MC. For the hydrophilic part, three materials were studied. Amorphous PEG_{20k}-$PLA_{7.5k}$ and crystalline PEG_{20k}-$PLLA_{7.5k}$ were prepared using $PEG_{8arm}20k$-$(PLA_{13})_8$-MC and $PEG_{8arm}20k$-$(PLLA_{13})_8$, respectively. Finally, to further increase the crystallinity of the resulting material, a film based on the stereo-complexation of PDLA and PLLA (PEG_{20k}-$PLLA_{7.5k}$/PEG_{20k}-$PDLA_{7.5k}$) was produced by mixing an equal mass of $PEG_{8arm}20k$-$(PLLA_{13})_8$-MC and $PEG_{8arm}20k$-$(PDLA_{13})_8$-MC.

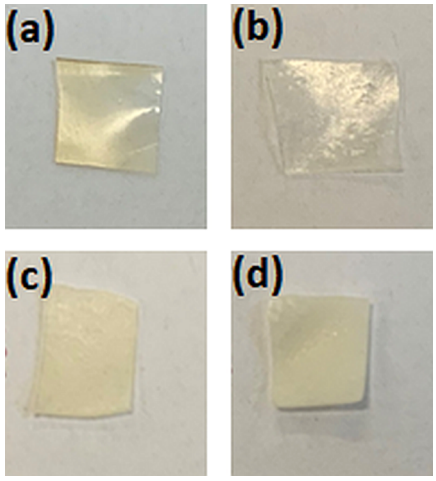

Figure 2. Visual aspect of the networks. Pictures of the different materials after crosslinking: (a) PEG_{10k}-PLA_{40k}, (b) PEG_{20k}-$PLA_{7.5k}$, (c) PEG_{20k}-$PLLA_{7.5k}$, and (d) PEG_{20k}-$PLLA_{7.5k}$/PEG_{20k}-$PDLA_{7.5k}$.

Before crosslinking, DSC analyses confirmed the higher degree of crystallinity of $PEG_{8arm}20k$-$(PLLA_{13})_8$-MC and $PEG_{8arm}20k$-$(PDLA_{13})_8$-MC compared to $PEG_{8arm}20k$-$(PLA_{13})_8$-MC, with increased melting temperature and fusion enthalpy (Table 2). The difference was however rather limited in agreement with a high EG/LA ratio and short PLA chains targeted for the hydrogel's precursors. Of note, even for amorphous PLA blocks, crystallinity is detected as a consequence of the crystallinity of the eight-armed PEG core that is still present despite the fact that crystallization is frustrated due to the star-block copolymer nature of the copolymers. This was confirmed by the comparison of the thermograms and of the enthalpies of melting of the eight-armed PEG macroinitiator and of the methacrylated copolymers (Figure S5). After irradiation, the differences were even less pronounced (Table 3) because of the crosslinking reducing the chain mobility, which could prevent the material from adopting a crystalline conformation.

After the solubilization of the polymers, the solutions were cast onto molds and let to dry in dark places before being irradiated under UV light to yield the films. Depending on the nature of the copolymers used to prepare the networks and their crystallinity, they ranged from translucid (copolymers

https://doi.org/10.1021/acsami.2c11264
ACS Appl. Mater. Interfaces 2022, 14, 43719−43731

Table 3. Crosslinking Efficiency Evaluated by Gel Fraction Analyses (300 μm Thick Films, 5 min UV Irradiation Per Side) and Thermal Properties of Crosslinked Materials[a]

sample	copolymer	gel fraction ± SD (%)	T_g (°C)	T_m (°C)	ΔH_m (J g^{-1})
PEG_{10k}-PLA_{40k}	$PEG_{8arm}10k$-$(PLA_{69})_8$-MC	93 ± 2	12.1	nd[b]	nd
PEG_{20k}-$PLA_{7.5k}$	$PEG_{8arm}20k$-$(PLA_{13})_8$-MC	97 ± 1	nd	25	−36.6
PEG_{20k}-$PLLA_{7.5k}$	$PEG_{8arm}20k$-$(PLLA_{13})_8$-MC	96 ± 0.5	nd	30	−38.5
PEG_{20k}-$PLLA_{7.5k}$ / PEG_{20k} − PDLA $_{7.5k}$	$PEG_{8arm}20k$-$(PLLA_{13})_8$-MC / $PEG_{8arm}20k$-$(PDLA_{13})_8$-MC	96 ± 0.5	nd	30	−31.4

[a]Data are expressed as means and correspond to measurements with n = 3. [b]Not detected under the conditions of analysis.

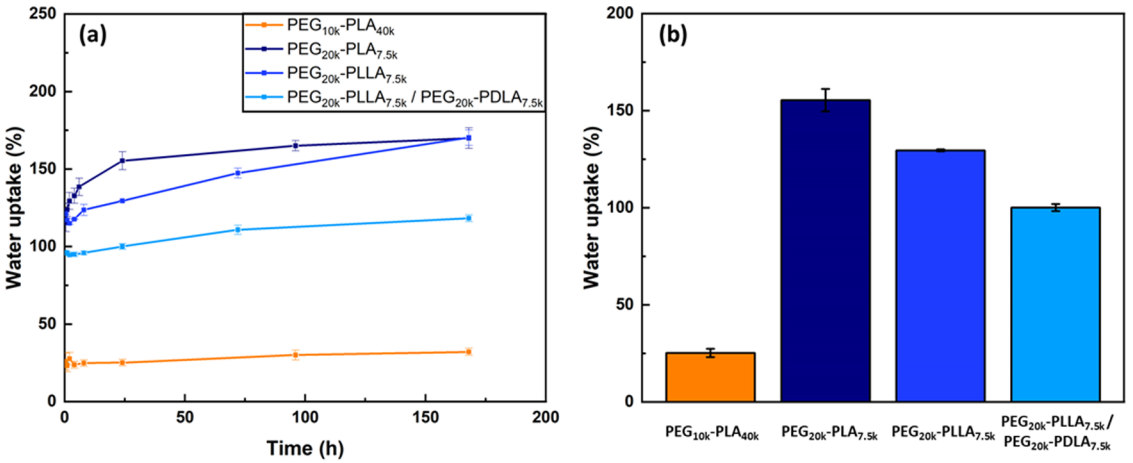

Figure 3. Water uptake of the networks. (a) Evolution of water uptake in PBS with time. (b) Water uptake after 24 h in PBS. Data are expressed as the mean ± SD and correspond to measurements with n = 3.

with amorphous PLA blocks, Figure 2a,b) to opaque films (copolymers with crystalline PLA blocks, Figure 2c,d).

All samples exhibited gel fractions exceeding 90% (Table 3), which confirmed the high crosslinking efficiency of the star-shaped polymers without the need to use photoinitiators. This is explained by the important reactivity of the copolymers that have a high number of methacrylate UV-reactive groups (8 per chain). PEG_{10k}-PLA_{40k} showed a slightly lower gel fraction (93%) compared to the other copolymers (≥96%), which can be explained by its higher molecular weight (50 000 vs 27 500 g mol^{-1}).

Finally, the crosslinking efficiency was further investigated through NMR spectroscopy with the objective to highlight the possible presence of residual methacrylate moieties after crosslinking. After being irradiated under UV light, one hydrophilic network (PEG_{20k}-$PLA_{7.5k}$) and one hydrophobic one (PEG_{10k}-PLA_{40k}) were selected and immersed in DCM for 24 h before analysis of the insoluble crosslinked parts by 1H HRMAS NMR. For PEG_{20k}-$PLA_{7.5k}$, the HRMAS NMR spectrum (Figure S6) showed no characteristic peaks of methacrylate groups, which demonstrated a high crosslinking efficiency. For PEG_{10k}-PLA_{40k}, low amounts of unreacted methacrylate groups (8%) were detected (Figure S7). This difference can be explained by the higher molecular mass of the copolymer and the increased chain length, which make the meeting between the chain ends more difficult. Of note, as these materials exhibited gel fractions similar to PEG_{20k}-$PLA_{7.5k}$ and were obtained from copolymers with the same molecular weight and EG/LA ratio, ^{1}H HRMAS NMR analyses were not performed on PEG_{20k}-$PLLA_{7.5k}$ and PEG_{20k}-$PLLA_{7.5k}$/PEG_{20k}-$PDLA_{7.5k}$.

As we chose to develop tubes that display self-rolling capacities mainly based on the difference in swelling between the two layers, it was essential to study the water uptake of the different networks prepared. The water uptake was monitored during a week (Figure 3a). After 24 h of immersion and for all of the samples, the water uptake started to reach a plateau, whose value is reported in Figure 3b. As expected, PEG_{10k}-PLA_{40k} showed a limited swelling ratio with a low value of 25%, which confirmed its potential to be used as the hydrophobic layer in the bilayer construct. All other networks exhibited high water swelling abilities that were modulated by the crystallinity of the copolymer. Indeed, the highest value of 155% was obtained for PEG_{20k}-$PLA_{7.5k}$, whereas crystalline PEG_{20k}-$PLLA_{7.5k}$ attained 130% and stereocomplexed PEG_{20k}-$PLLA_{7.5k}$/PEG_{20k}-$PDLA_{7.5k}$ only 100%. Of note, for the less crystalline copolymers, PEG_{20k}-$PLA_{7.5k}$ and PEG_{20k}-$PLLA_{7.5k}$, the limited residual swelling measured after 100 h could also be due to the starting degradation as shown by a weight loss around 10%. These behaviors were expected. The networks intended to be used as the hydrophilic layer displayed higher water absorption capacities compared to the networks dedicated to the hydrophobic layer. The significant difference in the swelling of the two layers should be responsible for the driving force enabling the spontaneous rolling of the tube.

3.3. Mechanical Properties of the Networks. As aforementioned, the mechanical properties are also a key parameter to lead to the inhomogeneous stress profile that will cause the self-rolling. Indeed, the hydrophobic layer should be stiffer compared to the hydrophilic one to assist in the rolling of the tube.

The mechanical properties of the networks were therefore assessed through a uniaxial tensile test performed not only in the dry state at room temperature but also in the hydrated state at 37 °C to mimic physiological conditions (Figure 4). The results are presented in Table 4. In the dry state and at room

https://doi.org/10.1021/acsami.2c11264
ACS Appl. Mater. Interfaces 2022, 14, 43719−43731

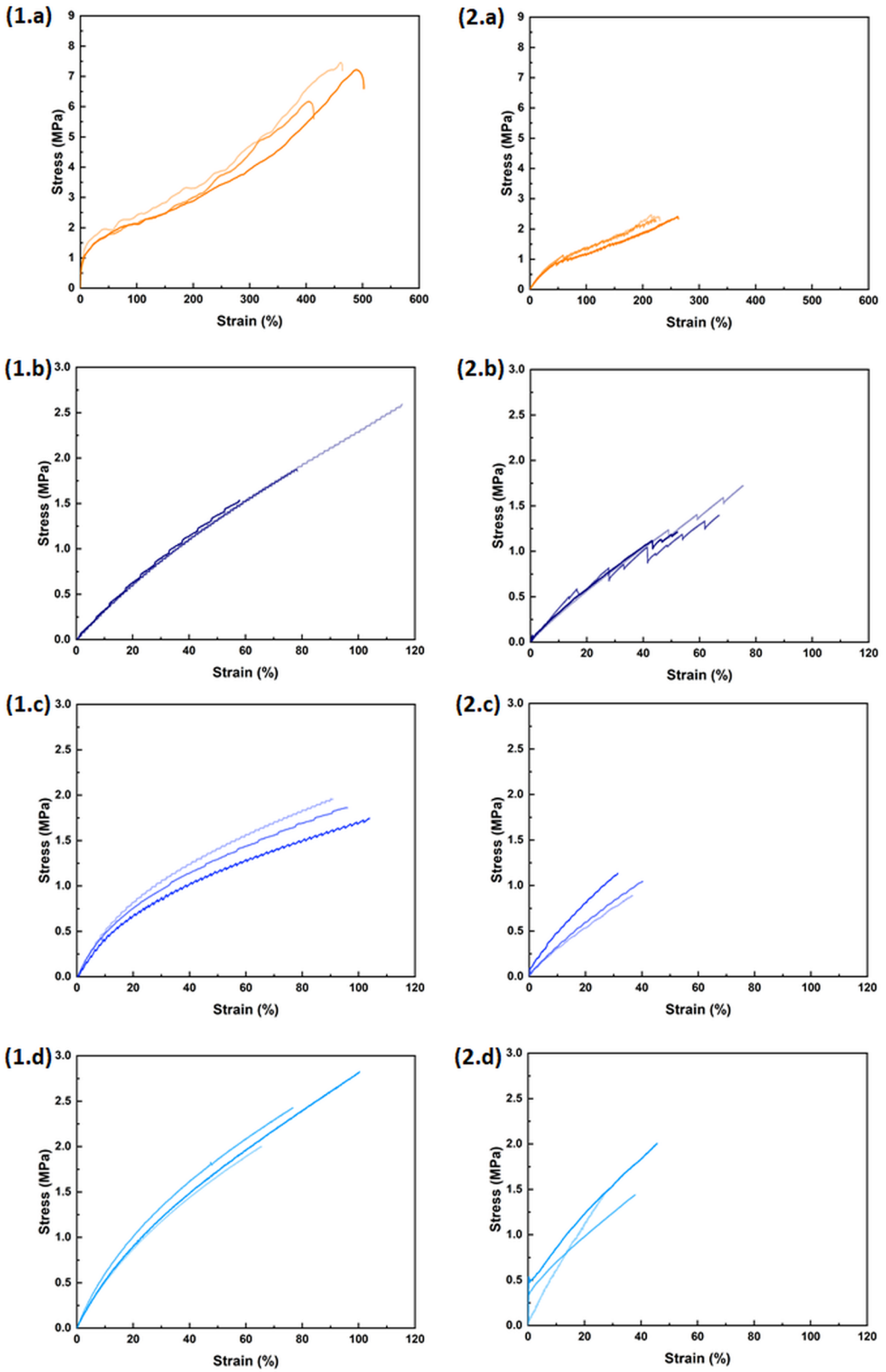

Figure 4. Mechanical evaluation of the networks by tensile tests. Stress−strain curves in the (1) dry state at room temperature and in the (2) hydrated state at 37 °C of (a) PEG_{10k}-PLA_{40k}, (b) PEG_{20k}-$PLA_{7.5k}$, (c) PEG_{20k}-$PLLA_{7.5k}$, and (d) PEG_{20k}-$PLLA_{7.5k}$/PEG_{20k}-$PDLA_{7.5k}$.

temperature, PEG_{10k}-PLA_{40k} showed high stress (σ_{break} = 6.5 MPa) and elongation at break (ε_{break} = 460%) compared to all of the hydrophilic candidates, which supported its choice as the stiffer layer. It also had a superior Young's modulus (E = 16.3 MPa) but exhibited a low elastic limit (ε_{yield} = 5%). In the hydrated state at 37 °C, the mechanical properties were

https://doi.org/10.1021/acsami.2c11264
ACS Appl. Mater. Interfaces 2022, 14, 43719−43731

Table 4. Mechanical Properties in the Dry State at Room Temperature and Hydrated State at 37 °C[a]

	dry state, room temperature					hydrated state, 37 °C				
sample	E (MPa)	σ_{yield} (MPa)	ε_{yield} (%)	σ_{break} (MPa)	ε_{break} (%)	E (MPa)	σ_{yield} (MPa)	ε_{yield} (%)	σ_{break} (MPa)	ε_{break} (%)
PEG_{10k}-PLA_{40k}	16.3 ± 3.4	1.0 ± 0.1	5 ± 1	6.5 ± 0.8	460 ± 44	2.4 ± 0.1	0.5 ± 0.1	19 ± 3	2.2 ± 0.1	239 ± 21
PEG_{20k}-$PLA_{7.5k}$	2.9 ± 0.3	0.5 ± 0.1	19 ± 2	2.0 ± 0.5	93 ± 20	3.1 ± 0.4	0.4 ± 0.1	13 ± 1	1.4 ± 0.3	65 ± 12
PEG_{20k}-$PLLA_{7.5k}$	5.0 ± 0.1	0.4 ± 0.1	9 ± 2	1.8 ± 0.2	94 ± 3	3.5 ± 0.8	0.3 ± 0.1	9 ± 1	1.0 ± 0.1	36 ± 4
PEG_{20k}-$PLLA_{7.5k}$ / PEG_{20k} − $PDLA_{7.5k}$	5.4 ± 0.8	0.6 ± 0.1	11 ± 2	2.4 ± 0.4	81 ± 18	4.6 ± 1.3	0.6 ± 0.1	6 ± 1	1.7 ± 0.3	37 ± 9

[a]Data are expressed as the mean ± SD and correspond to measurements with n = 3.

decreased but remained superior to the ones of hydrophilic samples. The stress at break reached 2.2 MPa, and the elongation at break reached 239%. Moreover, the Young's modulus decreased to 2.4 MPa and the elastic domain increased to 19%.

As expected, hydrophilic materials exhibited weaker mechanical properties. In the dry state and at room temperature, PEG_{20k}-$PLA_{7.5k}$, PEG_{20k}-$PLLA_{7.5k}$, and PEG_{20k}-$PLLA_{7.5k}$/PEG_{20k}-$PDLA_{7.5k}$ exhibited close elongations at break (93, 94, and 81%, respectively) and ultimate strains (2.0, 1.8, and 2.4 MPa, respectively). However, when looking at the elastic domain, the crystallinity of the materials impacted the behaviors. Indeed, amorphous PEG_{20k}-$PLA_{7.5k}$ displayed a Young's modulus of 2.9 MPa for an elastic limit of 19%. Due to their higher crystallinity, PEG_{20k}-$PLLA_{7.5k}$ and PEG_{20k}-$PLLA_{7.5k}$/PEG_{20k}-$PDLA_{7.5k}$ showed increased Young's moduli (5.0 and 5.4 MPa, respectively) with shorter elastic domains (9 and 11%, respectively). At 37 °C in the hydrated state, although the mechanical properties were reduced, the same trend was observed. The ultimate strains (between 1.0 and 1.7 MPa) and Young's moduli (between 3.1 and 4.6 MPa) were close for all samples with the more crystalline ones being slightly stiffer. The differences were more pronounced when comparing the strain behaviors. The materials with lower absorption capacities—i.e., the more crystalline ones—showed twice smaller elastic domains and elongations at break (ε_{yield} = 6 and 9% and ε_{break} = 36 and 39% for PEG_{20k}-$PLLA_{7.5k}$/PEG_{20k}-$PDLA_{7.5k}$ and PEG_{20k}-$PLLA_{7.5k}$, respectively) compared to PEG_{20k}-$PLA_{7.5k}$ (ε_{yield} = 13% and ε_{break} = 65%).

Additional cyclic tensile tests carried out under ambient conditions confirmed the previous results (Figure 5). The samples were submitted to nine cyclic loads at different strains (2, 5, and 15%), and the resilience was calculated for the final cycle. For all samples, the resilience was in accordance with their elastic limit (Table S1) with, for example, resilience superior to 89 at 15% strain for all of the hydrophilic copolymers and around 20% for the hydrophobic copolymer.

Finally, relaxation tests were performed to characterize the viscoelasticity of the different networks in the dry state (Figure 5). The hydrophobic layer PEG_{10k}-PLA_{40k} exhibited a viscous behavior with important relaxation within a few seconds. On the hydrophilic side, PEG_{20k}-$PLLA_{7.5k}$ behaved similarly, whereas PEG_{20k}-$PLA_{7.5k}$ and PEG_{20k}-$PLLA_{7.5k}$/PEG_{20k}-$PDLA_{7.5k}$ did not relax or barely, which confirmed their elastic behavior (Table S2). For the stereocomplexed PEG_{20k}-$PLLA_{7.5k}$/PEG_{20k}-$PDLA_{7.5k}$, it can be explained by the crosslinking density and the presence of physical nodes of crystallinity. In the case of PEG_{20k}-$PLA_{7.5k}$, which showed the highest gel fraction and resilience, it can be due to its high crosslink density.

This set of results confirms that the hydrophobic and hydrophilic networks possess significantly different mechanical behaviors, which should contribute in generating the inhomogeneous stress profile that will lead to the spontaneous rolling of the tube.

3.4. Bilayered Construct Preparation and Self-Rolling.

Following the validation of the mechanical properties and swelling properties of each material individually, they have been combined to prepare the targeted bilayered constructs. Each hydrophilic network has been associated with the hydrophobic one. The samples were all prepared following the same protocol consisting of two consecutive solvent evaporation steps before UV light irradiation on both sides to ensure a homogeneous crosslinking (Figure 6a). Each time, the same mass of polymers was used for the hydrophobic and hydrophilic parts. Regardless of the composition, bilayered constructs with a thickness of about 500 μm were obtained.

Not only the influence of the nature of the hydrophilic layer on the self-rolling process was investigated but also the impact of the shape of the samples. Therefore, three types of shapes were selected and tested: a square of 1 cm × 1 cm, a short rectangle of 0.5 cm × 1 cm, and a long rectangle of 0.5 cm × 1.5 cm (Figure 6b). After being cut at the appropriate dimensions, the samples were immersed in water at 37 °C and the rolling was followed visually for 1.5 min. The results are presented in Figure 6.

All of the samples showed a spontaneous curvature when immersed in water. However, the nature of the hydrophilic part of the bilayer construct impacted the efficiency of the phenomenon. Indeed, when PEG_{20k}-$PLA_{7.5k}$ was used, it led to a tube with a multilayered wall and a diameter of approximately 2 mm regardless of the initial shape of the sample (Figure 6f). On the contrary, with PEG_{20k}-$PLLA_{7.5k}$, only bending was observed. It was also demonstrated that the dimension of the material affected the rolling since with the mix of PEG_{20k}-$PLLA_{7.5k}$ and PEG_{20k}-$PDLA_{7.5k}$, tubes formed only with the rectangle samples and not with the square. In this case, larger tubes with a diameter of about 3−4 mm with a single wall were obtained. Moreover, it is important to note that regardless of the construct, no delamination between the layers was observed, which can be explained by the good affinity and the covalent crosslinking between the polymer layers. Finally, the rolling was reversible upon dehydration as shown in Figure S8. Short rectangle samples were self-rolled and then let to dry at room temperature. The construct based on PEG_{20k}-$PLA_{7.5k}$, which formed a full tube, was able to unroll and recover its initial shape after 2 h. With PEG_{20k}-$PLLA_{7.5k}$ and PEG_{20k}-$PLLA_{7.5k}$/PEG20k-$PDLA_{7.5k}$, with the unrolling occurred faster as the samples were initially only bent. Of note, the best results (Movie S1) were obtained with PEG_{20k}-$PLA_{7.5k}$, the hydrophilic layer presenting the highest resilience

https://doi.org/10.1021/acsami.2c11264
ACS Appl. Mater. Interfaces 2022, 14, 43719−43731

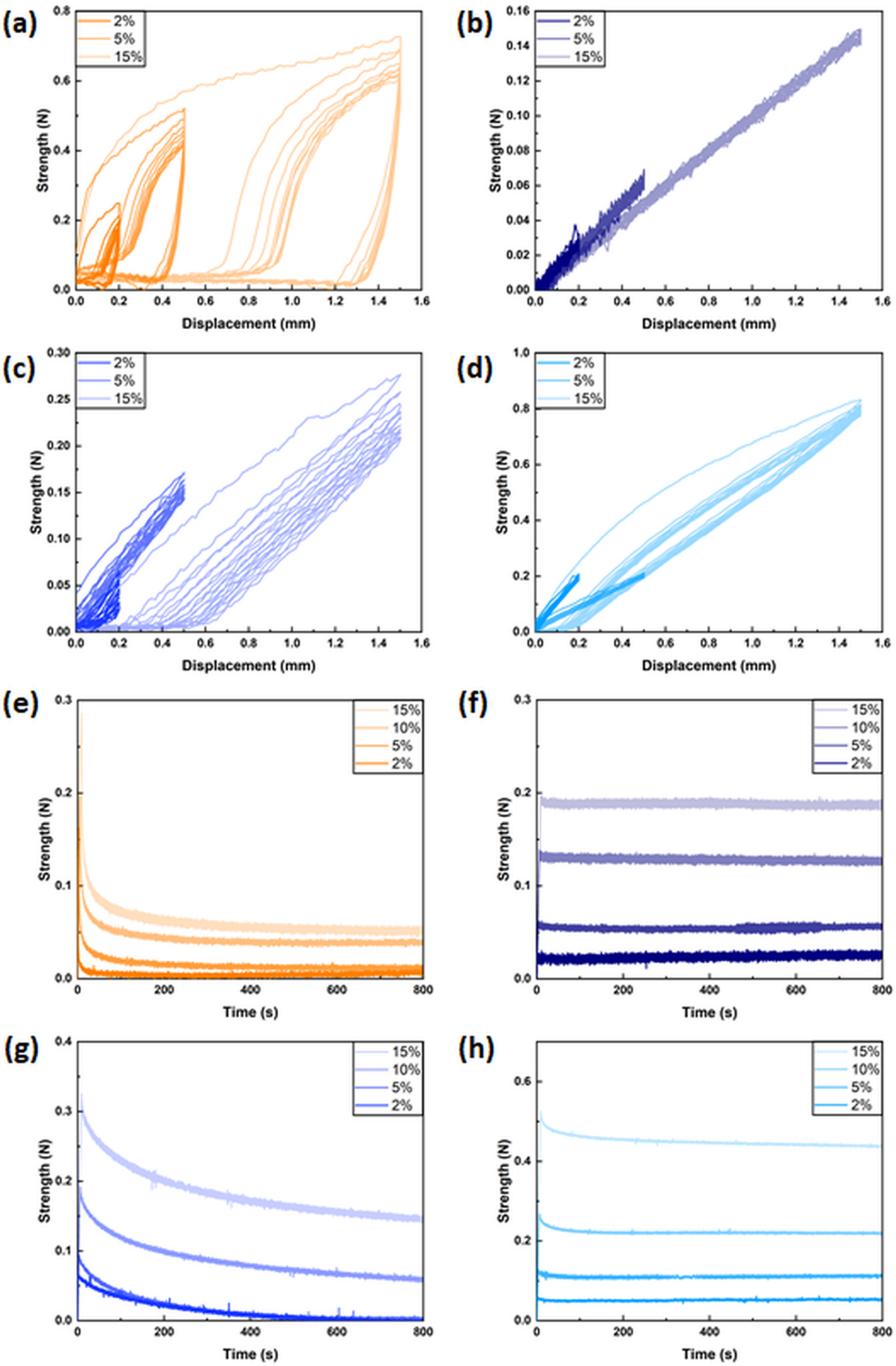

Figure 5. Mechanical evaluation of the networks under cyclic loads and relaxation test. Cyclic load curves at 2, 5, and 15% of deformation for (a) PEG_{10k}-PLA_{40k}, (b) PEG_{20k}-$PLA_{7.5k}$, (c) PEG_{20k}-$PLLA_{7.5k}$, and (d) PEG_{20k}-$PLLA_{7.5k}$/PEG_{20k}-$PDLA_{7.5k}$. Relaxation curves at 2, 5, 10, and 15% of deformation for (e) PEG_{10k}-PLA_{40k}, (f) PEG_{20k}-$PLA_{7.5k}$, (g) PEG_{20k}-$PLLA_{7.5k}$, and (h) PEG_{20k}-$PLLA_{7.5k}$/PEG_{20k}-$PDLA_{7.5k}$.

and the lowest relaxation, that is, the hydrophilic network with the most elastomeric behavior. The tube formed in less than 30 s, which is fast compared to what can be found in the literature, where some works reported tube rolling times ranging from a few minutes (5−25 min)[17,18] to many hours,[16] for systems based on degradable copolymers. This fast rolling could

https://doi.org/10.1021/acsami.2c11264
ACS Appl. Mater. Interfaces 2022, 14, 43719−43731

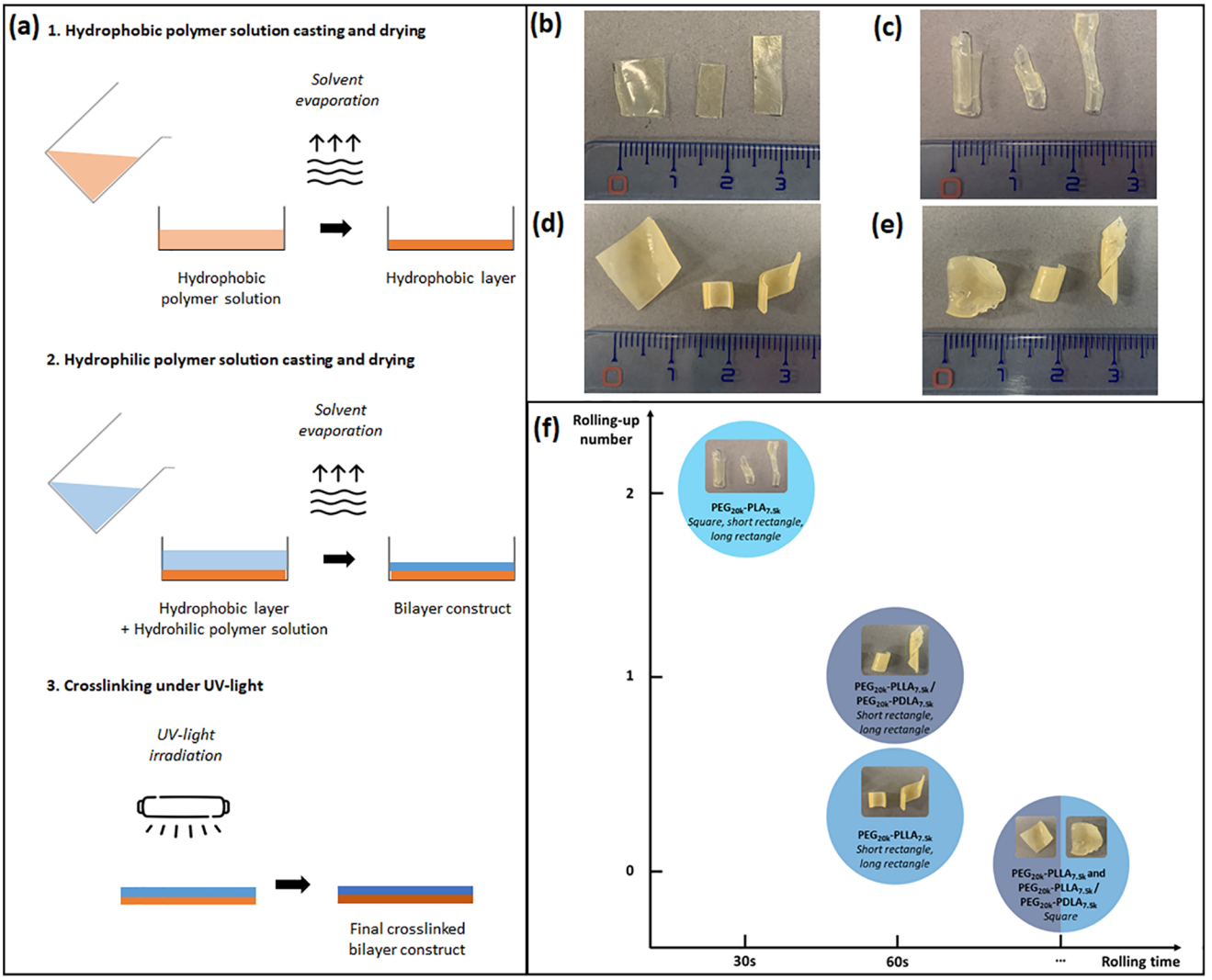

Figure 6. Preparation and characterization of self-rolling of the bilayered constructs. (a) Schematic representation of the bilayer construct preparation. Samples (b) PEG_{20k}-$PLA_{7.5k}$ before self-rolling and (c) PEG_{20k}-$PLA_{7.5k}$, (d) PEG_{20k}-$PLLA_{7.5k}$, and (e) PEG_{20k}-$PLLA_{7.5k}$/PEG_{20k}-$PDLA_{7.5k}$ after self-rolling. (f) Comparison of rolling properties of bilayered constructs upon immersion in water.

advantageously be used in the frame of the development of implantable medical devices, where a sterile flat construct could be rapidly turned into a tube upon hydration in the operating room without extending the duration of the intervention.

A fluorescent version of the best construct was prepared (see details in the supporting data) with the objective to clearly identify the layers in the construct, visualize the interface, and confirm the rolling direction. The hydrophobic and hydrophilic copolymers were fluorescently labeled with rhodamine B isothiocyanate and FITC, respectively, before being functionalized with methacrylate groups. Small amounts of fluorescent copolymers were then mixed with nonfluorescent PEG_{8arm}10k-$(PLA_{69})_8$-MC and PEG_{8arm}20k-$(PLA_{13})_8$-MC. Therefore, a colored and fluorescent bilayered construct composed of pink PEG_{10k}-PLA_{40k} and yellow PEG_{20k}-$PLA_{7.5k}$ was obtained (Figure 7a) and permitted us to confirm that the hydrophilic layer is the outer diameter of the rolled tube (Figure 7c). This was further demonstrated using FTIR spectroscopy. Indeed, as shown in Figure 7d, the FTIR spectrum of the inner diameter of the tube corresponds to PEG_{10k}-PLA_{40k}, whereas the FTIR spectrum of the outer diameter matches with PEG_{20k}-$PLA_{7.5k}$. In more detail, the absorption band of CO stretching (1750 cm^{-1}) of the PLA ester bond is predominant in the hydrophobic inner layer, whereas the absorption band corresponding to the CH stretching (2870 cm^{-1}) in PEG is dominating in the hydrophilic outer layer.

As explained in Section 3.1, star-shaped copolymers with a similar structure and methacrylate moieties were chosen to ensure a covalent association and cohesion between the layers. This was validated with the interface being visualized in orange and the gradual color change between the yellow and pink layers (Figure 7a), confirming a continuum between the layers without a discrete interface and a gradual shift from one layer to the other. It was also confirmed by SEM images of the rolled tube (Figure 7e,f) with no visible demarcation between the hydrophilic and hydrophobic layers.

Thus, by playing with the nature of the hydrophilic layer and the shape of the samples and by ensuring a gradual interface, thanks to the selection of two polymers of the same nature, we designed bilayered constructs that exhibit rapid and spontaneous self-rolling when immersed in water.

3.5. Degradation and Cytocompatibility. In view of future biomedical applications as temporary biomaterials, the

https://doi.org/10.1021/acsami.2c11264
ACS Appl. Mater. Interfaces 2022, 14, 43719−43731

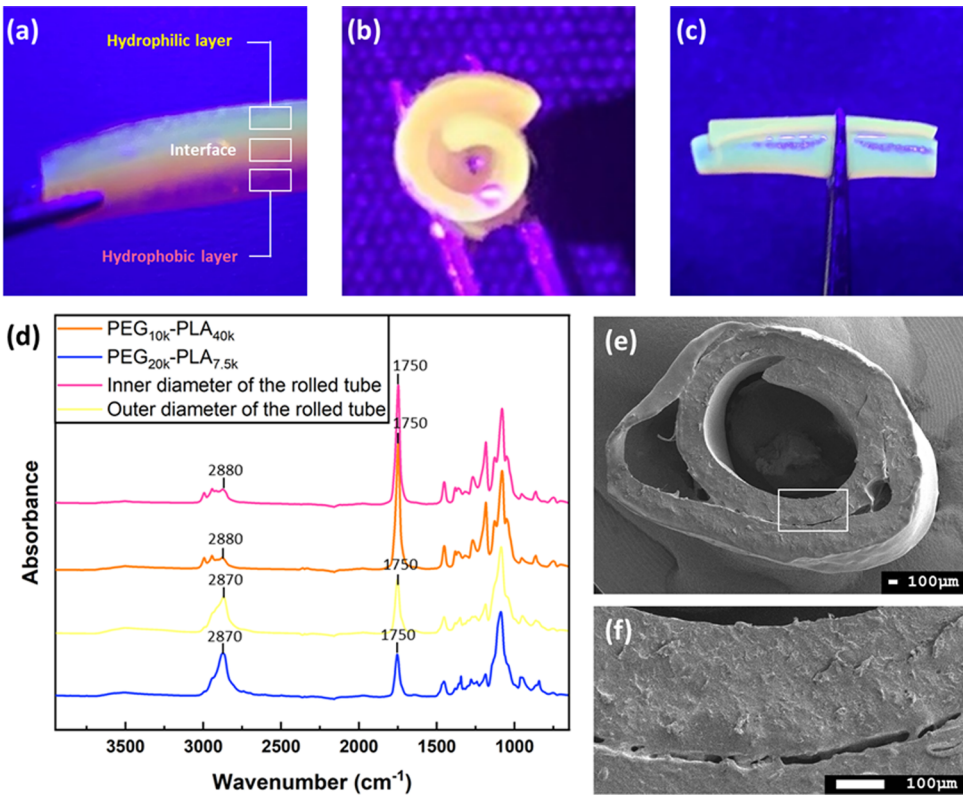

Figure 7. Confirmation of the structure of the self-rolled tubes. Fluorescent version of the bilayered construct composed of PEG_{10k}-PLA_{40k} (pink layer) and PEG_{20k}-$PLA_{7.5k}$ (yellow layer) (a) before and (b, c) after immersion and swelling in water. (d) FTIR spectra of PEG_{10k}-PLA_{40k}, PEG_{20k}-$PLA_{7.5k}$, and of the inner and outer layers of the rolled tube. (e) SEM image of the self-rolled bilayered construct. (f) SEM image of the cross-section of the self-rolled bilayered construct.

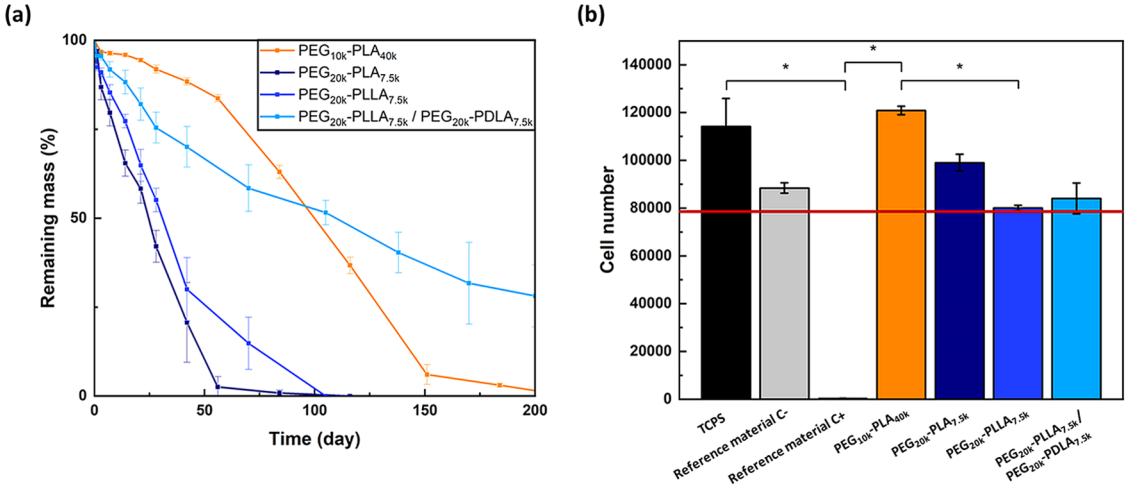

Figure 8. Degradation and cytocompatibility of the networks. (a) Evaluation of sample degradation in PBS (pH 7.4) at 37 °C. Data are expressed as the mean ± SD and correspond to measurements with $n = 3$. (b) Cell viability evaluation assessed on L929 cells after treatment with an extract of polymer films for 24 h. Data are expressed as the mean ± SD and correspond to measurements with $n = 3$. Statistical analysis use a Kruskal–Wallis test followed by a Dunn post-hoc test (threshold of significance $^*p < 0.05$).

degradation of each type of photo-crosslinked network was investigated by monitoring their mass loss when immersed in PBS at 37 °C (Figure 8a). As expected, because of its higher hydrophobicity and limited swelling ratio, PEG_{10k}-PLA_{40k} showed the slowest initial degradation. However, once the samples were fragmented (after 56 days), the degradation rate increased until their total disappearance after 216 days. On the contrary, the other networks, due to their hydrophilicity, showed much faster initial mass loss. Their degradation rate was in accordance with their crystallinity and water absorption. PEG_{20k}-$PLA_{7.5k}$, with amorphous PLA blocks and a higher swelling capacity, degraded the fastest with 50% weight loss after only 25 days and almost full degradation after 55 days. The crystalline PEG_{20k}-$PLLA_{7.5k}$ showed a similar initial degradation that slowed down to the end to reach full degradation after 100 days. This is attributed to the fast initial degradation of the amorphous parts of the network that leaves only the most crystalline parts to be degraded in the later stage.

https://doi.org/10.1021/acsami.2c11264
ACS Appl. Mater. Interfaces 2022, 14, 43719–43731

Finally, the stereocomplexed network PEG_{20k}-$PLLA_{7.5k}$/PEG_{20k}-$PDLA_{7.5k}$ showed a much slower degradation compared to the other hydrophilic networks. It displayed a late fragmentation (appearing after 138 days) and a slow degradation with a quasilinear weight loss profile leading to only 60% loss after 150 days. This slower degradation may be of interest to develop self-rolling tubes made of layers exhibiting degradation times in the same range, which could ensure good conservation of the tube's rolled shape in time.

We finally evaluated the potential of different crosslinked networks for use in cell-contacting applications. Therefore, the cytotoxicity of the individual materials was assessed on extracts following ISO 10993-12 recommendations. Even if PEG and PLA have already been approved by the Food and Drug Administration, the multifunctionalization may induce cytotoxicity. The extracts from polymer films or reference materials C− and C+ were added on L929 fibroblasts seeded into well, and cell viability was evaluated over a 24 h period (Figure 8b). Only extracts from positive control films (C+) gave 0% cell viability on L929 cells. The extracts from all of the individual crosslinked networks led to viability on L929 cells above 70%. These results highlight the noncytotoxicity of PEG_{10k}-PLA_{40k}, PEG_{20k}-$PLA_{7.5k}$, PEG_{20k}-$PLLA_{7.5k}$, and PEG_{20k}-$PLLA_{7.5k}$/PEG_{20k}-$PDLA_{7.5k}$ that could be further considered for biomedical applications.

4. CONCLUSIONS

In this work, we designed self-rolling tubes made of biodegradable bilayered constructs that exhibit spontaneous actuation when immersed in water. Self-rolling was obtained from the differences of mechanical and swelling properties of two photo-crosslinked layers. To this end, we synthesized hydrophobic or hydrophilic PEG-PLA star-shaped copolymers functionalized with methacrylate groups at their chain ends. The high number of photo-reactive moieties led to high gel fractions superior to 90% without a photoinitiator. The hydrophobic layer based on PEG_{10k}-PLA_{40k} showed a swelling limited to 25% and a plastic behavior, whereas the hydrophilic layer had a swelling of up to 155% and presented an elastomeric behavior when the amorphous PEG_{20k}-$PLA_{7.5k}$ or stereocomplexed PEG_{20k}-$PLLA_{7.5k}$/PEG_{20k}-$PDLA_{7.5k}$ was used. The concomitant UV irradiation of the two layers resulted in a bilayered film able to self-roll in water in less than 30 s depending on the nature of the hydrophilic layer and on the shape of the sample. Finally, the cytocompatibility and the degradability (ranging from 25 days to over 150 days for PEG_{20k}-$PLA_{7.5k}$ and stereocomplexed PEG_{20k}-$PLLA_{7.5k}$/PEG_{20k}-$PDLA_{7.5k}$, respectively) of these networks were confirmed. Overall, the present work highlights the importance of a sound design (polymers of the same nature, cohesive/gradual interface) to ensure a fast actuation. We believe that it opens the way toward useful self-rolling resorbable materials for biomedical applications and that further optimizations in terms of the layer thicknesses and hydrophilicities or of the sample shape would result in even faster and tighter self-rolling systems. In particular, it would be interesting to work on the processing and replace the solvent casting technique by a method (e.g., spin-coating) that could make it possible to precisely control the thickness and obtain more uniform constructs.

ASSOCIATED CONTENT

Supporting Information

The Supporting Information is available free of charge at https://pubs.acs.org/doi/10.1021/acsami.2c11264.

^{1}H NMR spectrum of star-shaped PEG-PLA copolymers; SEC analysis before and after methacrylate chain-end functionalization; synthetic scheme of methacrylate functional copolymers and ^{1}H NMR spectrum of PEG_{8arm}-PLA-MC; ^{1}H DOSY NMR spectrum of methacryloyl chloride and methacrylate functional PEG-PLA copolymer; DSC thermograms of PEG_{8arm}20k, PEG_{8arm}20k-$(PLA_{13})_8$-MC, PEG_{8arm}20k-$(PLLA13)_8$-MC, and PEG_{8arm}20k-$(PDLA_{13})_8$-MC (second heating ramp); ^{1}H HRMAS NMR spectrum of insoluble fraction of PEG_{20k}-$PLA_{7.5k}$; ^{1}H HRMAS NMR spectrum of insoluble fraction of PEG_{10k}-PLA_{40k}; unrolling upon dehydration at room temperature; resilience (%) at different strains (2, 5, and 15%) in dry state at room temperature; relaxation (%) at different strains (2, 5, 10, and 15%) in dry state at room temperature (PDF)

Real-time movie of self-rolling; and preparation of the fluorescent bilayered construct (AVI)

AUTHOR INFORMATION

Corresponding Author

Benjamin Nottelet − *Polymers for Health and Biomaterials, IBMM, Univ Montpellier, CNRS, ENSCM, 34090 Montpellier, France;* orcid.org/0000-0002-8577-9273; Email: benjamin.nottelet@umontpellier.fr

Authors

Mathilde Grosjean − *Polymers for Health and Biomaterials, IBMM, Univ Montpellier, CNRS, ENSCM, 34090 Montpellier, France*

Sidzigui Ouedraogo − *Université de Haute-Alsace, CNRS, 68100 Mulhouse, France*

Stéphane Déjean − *Polymers for Health and Biomaterials, IBMM, Univ Montpellier, CNRS, ENSCM, 34090 Montpellier, France*

Xavier Garric − *Polymers for Health and Biomaterials, IBMM, Univ Montpellier, CNRS, ENSCM, 34090 Montpellier, France; Department of Pharmacy, Nîmes University Hospital, 30900 Nimes, France*

Valeriy Luchnikov − *Université de Haute-Alsace, CNRS, 68100 Mulhouse, France;* orcid.org/0000-0003-1740-4899

Arnaud Ponche − *Université de Haute-Alsace, CNRS, 68100 Mulhouse, France*

Noëlle Mathieu − *Institute for Radioprotection and Nuclear Safety, IRSN, 92260 Fontenay-aux-Roses, France*

Karine Anselme − *Université de Haute-Alsace, CNRS, 68100 Mulhouse, France*

Complete contact information is available at: https://pubs.acs.org/10.1021/acsami.2c11264

Author Contributions

M.G.: Investigation, writing—original draft; S.O.: investigation; S.D.: investigation; X.G.: visualization; V.L.: conceptualization, writing review; A.P.: conceptualization, writing review; N.M.: conceptualization, writing review, funding acquisition, project administration; K.A.: conceptualization, writing review,

funding acquisition, project administration; and B.N.: conceptualization, writing—original draft, writing review and editing, funding acquisition, supervision, and project administration.

Notes

The authors declare no competing financial interest.

■ ACKNOWLEDGMENTS

This work was supported by the ANR2019-OPENN held by the University of Montpellier (ANR-19-CE19-0022-02), CNRS (ANR-19-CE19-0022-03), IRSN (ANR-19-CE19-0022-01), Institut Carnot Chimie Balard Cirimat, and Institut Carnot MICA (COROL-2019). The authors thank Cédric Totée from the Institut Charles Gerhardt Montpellier (ICGM) for the HRMAS experiments.

■ REFERENCES

(1) Zhao, W.; Liu, L.; Zhang, F.; Leng, J.; Liu, Y. Shape Memory Polymers and Their Composites in Biomedical Applications. *Mater. Sci. Eng., C* **2019**, *97*, 864−883.
(2) Fratzl, P.; Barth, F. G. Biomaterial Systems for Mechanosensing and Actuation. *Nature* **2009**, *462*, 442−448.
(3) Vakil, A. U.; Petryk, N. M.; Shepherd, E.; Monroe, M. B. B. Biostable Shape Memory Polymer Foams for Smart Biomaterial Applications. *Polymers* **2021**, *13*, No. 4084.
(4) Hardy, J. G.; Palma, M.; Wind, S. J.; Biggs, M. J. Responsive Biomaterials: Advances in Materials Based on Shape-Memory Polymers. *Adv. Mater.* **2016**, *28*, 5717−5724.
(5) Keller, A.; Warren, H. In Het. Development of a Facile One-Pot Synthesis Method for an Ingestible PH Sensitive Actuator. *MRS Adv.* **2020**, *5*, 881−889.
(6) Luchnikov, V.; Kumar, K.; Stamm, M. Toroidal Hollow-Core Microcavities Produced by Self-Rolling of Strained Polymer Bilayer Films. *J. Micromech. Microeng.* **2008**, *18*, No. 035041.
(7) Luchnikov, V.; Stamm, M. Self-Rolled Polymer Microtubes with Engineered Hidden Walls. *Phys. E* **2007**, *37*, 236−240.
(8) Hu, Z.; Zhang, X.; Li, Y. Synthesis and Application of Modulated Polymer Gels. *Science* **1995**, *269*, 525−527.
(9) Liu, L.; Ghaemi, A.; Gekle, S.; Agarwal, S.; Liu, L.; Agarwal, S.; Ghaemi, A.; Gekle, S. One-Component Dual Actuation: Poly-(NIPAM) Can Actuate to Stable 3D Forms with Reversible Size Change. *Adv. Mater.* **2016**, *28*, 9792−9796.
(10) Liu, L.; Jiang, S.; Sun, Y.; Agarwal, S. Giving Direction to Motion and Surface with Ultra-Fast Speed Using Oriented Hydrogel Fibers. *Adv. Funct. Mater.* **2016**, *26*, 1021−1027.
(11) Simpson, B.; Nunnery, G.; Tannenbaum, R.; Kalaitzidou, K. Capture/Release Ability of Thermo-Responsive Polymer Particles. *J. Mater. Chem.* **2010**, *20*, 3496−3501.
(12) Zakharchenko, S.; Puretskiy, N.; Stoychev, G.; Stamm, M.; Ionov, L. Temperature Controlled Encapsulation and Release Using Partially Biodegradable Thermo-Magneto-Sensitive Self-Rolling Tubes. *Soft Matter* **2010**, *6*, 2633−2636.
(13) Park, J. Y.; Oh, H. J.; Kim, D. J.; Baek, J. Y.; Lee, S. H. A Polymeric Microfluidic Valve Employing a PH-Responsive Hydrogel Microsphere as an Actuating Source. *J. Micromech. Microeng.* **2006**, *16*, No. 656.
(14) Luchnikov, V.; Sydorenko, O.; Stamm, M. Self-Rolled Polymer and Composite Polymer/Metal Micro- And Nanotubes with Patterned Inner Walls. *Adv. Mater.* **2005**, *17*, 1177−1182.
(15) Luchnikov, V.; Lonov, L.; Stamm, M. Self-Rolled Polymer Tubes: Novel Tools for Microfluidics, Microbiology, and Drug-Delivery Systems. *Macromol. Rapid Commun.* **2011**, *32*, 1943−1952.
(16) Zakharchenko, S.; Sperling, E.; Ionov, L. Fully Biodegradable Self-Rolled Polymer Tubes: A Candidate for Tissue Engineering Scaffolds. *Biomacromolecules* **2011**, *12*, 2211−2215.
(17) Stroganov, V.; Zakharchenko, S.; Sperling, E.; Meyer, A. K.; Schmidt, O. G.; Ionov, L. Biodegradable Self-Folding Polymer Films with Controlled Thermo-Triggered Folding. *Adv. Funct. Mater.* **2014**, *24*, 4357−4363.
(18) Peng, L.; Zhu, J.; Agarwal, S. Self-Rolled Porous Hollow Tubes Made up of Biodegradable Polymers. *Macromol. Rapid Commun.* **2017**, *38*, No. 1700034.
(19) Buwalda, S. J.; Nottelet, B.; Coudane, J. Robust & Thermosensitive Poly(Ethylene Glycol)-Poly(ε-Caprolactone) Star Block Copolymer Hydrogels. *Polym. Degrad. Stab.* **2017**, *137*, 173−183.
(20) Gangolphe, L.; Déjean, S.; Bethry, A.; Hunger, S.; Pinese, C.; Garric, X.; Bossard, F.; Nottelet, B. Degradable Multi(Aryl Azide) Star Copolymer as Universal Photo-Crosslinker for Elastomeric Scaffolds. *Mater. Today Chem.* **2019**, *12*, 209−221.
(21) Buwalda, S. J.; Dijkstra, P. J.; Feijen, J. In Situ Forming Stereocomplexed and Post-Photocrosslinked Acrylated Star Poly-(Ethylene Glycol)-Poly(Lactide) Hydrogels. *Eur. Polym. J.* **2017**, *94*, 152−161.

https://doi.org/10.1021/acsami.2c11264
ACS Appl. Mater. Interfaces 2022, 14, 43719−43731